2,2-Biphenol-based Ultrathin Microporous Nanofilms for Highly Efficient Molecular Sieving Separation

RESEARCH ARTICLE

2,2'-Biphenol-based Ultrathin Microporous Nanofilms for Highly Efficient Molecular Sieving Separation

Shao-Lu Li, Guoliang Chang, Yangzheng Huang, Ken Kinooka, Yanting Chen, Wenming Fu, Genghao Gong,* Tomohisa Yoshioka, Neil B. McKeown,* and Yunxia Hu*

A. Prof. S.-L. Li, G. Chang, Y. Huang, Y. Chen, W. Fu, Prof. G. Gong, Prof. Y. Hu
State Key Laboratory of Separation Membranes and Membrane Processes
School of Materials Science and Engineering, Tiangong University
Tianjin 300387, P.R. China Tianjin 300387, P.R. China
E-mail: gonggenghao@tiangong.edu.cn, yunxiahu@tiangong.edu.cn
Mr. K. Kinooka, Prof. T. Yoshioka
Research Center for Membrane and Film Technology
Graduate School of Science, Technology and Innovation
Kobe University, Kobe 657-8501, Japan
Prof. N. B. McKeown
EaStCHEM, School of Chemistry,
University of Edinburgh, Scotland EH9 3FJ, UK.
E-mail: Neil.McKeown@ed.ac.uk

Supporting information for this article is given via a link at the end of the document.

Abstract: Organic solvent nanofiltration (OSN) is an emerging membrane separation technology, which urgently requires robust, easily processed, OSN membranes possessing high permeance and small solutes-selectivity to faciliate enhanced industrial uptake. Herein, we describe the use of two 2,2'-biphenol (BIPOL) derivatives with multiple reactive sites to fabricate hyper-crosslinked, microporous polymer nanofilms through interfacial polymerization (IP). Ultra-thin, defect-free polyesteramide/polyester nanofilms (~5 nm) could be obtained readily which can be ascribed to the relatively large molecular size and ionized nature of the phenol groups of the BIPOL monomers retarding the rate of the IP. The enhanced microporosity arisis from the hyper-crosslinked network structure and monomer rigidity. Specifically, the amino-BIPOL/PAN membrane exhibits extraordinary permselectivity performances with molecular weight cut-off as low as 233 Da and MeOH permeance of ~13 LMH/bar. Precise separation of small dye mixtures with similar molecular weights based on both their charge and molecular size are achieved.

Introduction

Membrane-based separation techniques have proven applications in the field of waste-water reclamation, sea water desalination and gas separations due to their high efficiency, less energy consumption and environmentally friendly chracteristics.[1] Of growing importance is the contribution of membranes to processes in chemical manufacture. For example, membranes for organic solvent nanofiltration (OSN), also referred to as solvent-resistant nanofiltration (SRNF), which can separate efficiently molecules of 200-1000 Da from organic solvent, have great potential for solvent recovery, separation of crude-oil mixtures, fractionation, separation of catalysts, and the purification of active pharmaceutical ingredients (APIs).[2]

However, OSN membranes with a combination of high solvent permeability, good solute selectivity, robust and scalability are required to extend the role of OSN technology in industry.[3] Thin-film composite (TFC) and integrally skin asymmetric (ISA) membranes are the two dominant OSN membrane types in current use. Notably, TFC membrane fabrication can separately adjust the microstructure, thickness of the top selective layer and the porous substrate, thus providing membranes with performances tailored to the specific application. The well-established technique of interfacial polymerization (IP) allows efficient fabrication of cross-linked polymeric nanofilms in situ on porous support and is used extensively for making polyamide desalination membranes. These IP nanofilms have been shown to exhibit good stability toward a range of organic solvents with different polarities.[4] In addition, it should be noted that the surface morphology, thickness, crosslinking degree, polymer network polarity, inner pore size and pore distribution of the thin-film selective layer all influence the separation performances of the resulting composite membranes.[5]

Many approaches have been developed to fabricate highly permeable TFC OSN membranes in recent years.[3d, 3e] Firstly, reducing the thickness of the selective layer is an obvious strategy that can greatly boost membrane permeances due to the shorter mass transport route,[6] such as the sub–10 nm polyamide nanofilms prepared on sacrificial nanostrands[7] and diamond like-carbon nanosheets membranes.[8] Secondly, the integration of highly porous nanofillers such as covalent organic frameworks (COFs),[9] metal-organic frameworks (MOFs)[10] and porous aromatic frameworks (PAFs)[11] into the selective layer. For these nanocomposite (TFN) membranes, the channels provided by the porous host can significantly promote solvent permeance, but at the cost of problems associated with filler aggregation and polymer-host incompatibility that can induce large voids that reduces membrane selectivity.[12] As a consequence, microporous network polymers fabricated by *in situ* polymerizations have emerged as the most promising method of producing the membrane selective layer including those based on conjugated microporous polymers (CMPs),[13] COFs,[14] and cross-linked versions of polymers of intrinsic microporosity (PIMs),[15] all of which can potentially provide separation performances with ultra-high solvent permeances and good selectivity.[16] Among the above strategies to fabricate advanced microporous organic polymers (MOPs) membranes, applying novel monomers for in-situ IP seems a more attractive and

promising strategy due to the potential of producing ultra-thin active layers using a process for which large-scale commercial membrane preparation is proven.[3e, 10c]

The fabrication of OSN membranes with high solute selectivity, and/or molecular-level precise separation is particularly attractive for replacing traditional purification technologies for chemical processing.[13a, 17] For instance, OSN membrane that can discriminate between solvent and molecules of around 300 Da will be important for solution concentration, purification and isolation of active pharmaceutical ingredients (APIs).[2b] However, most of the reported OSN membranes with high permeances only exhibited moderate rejections to small organic solutes, usually with larger molecular weight cut-off (MWCO > 350 Da).[18] In our recent work,[19] we employed a contorted BINOL-based monomer (7,7′-dihydroxy-2,2′-binaphthol) to fabricate a thin (~17 nm) polyarylate microporous polymer TFC OSN membrane, which exhibited very high organic solvent permeance, but showed only moderate solute rejections (with MWCO ~ 400 Da).

Herein, we describe the use of 5,5’-diamino-2,2′-biphenol (amino-BIPOL) and 6,6’-dihydroxyl-2,2’-biphenol (hydroxyl-BIPOL) with enhanced amide/ester forming functionality (Figure 1), which were designed to form IP polyesteramide/polyester nanofilms with smaller pore size when reacted with trimesoyl chloride (TMC), relative to those from the bifunctional BINOL.[20] The thickness of the as-fabricated cross-linked polyesteramide nanofilms from amino-BIPOL are as little as ~5 nm, with exceptional OSN separation performance of high solutes selectivity (MWCO ~233 Da) combined with and MeOH permeance of ~13 LMH/bar. The resulting polyester composite membrane from hydroxyl-BIPOL show MeOH permeance of ~17.2 LMH/bar and with MWCO of 314 Da. Importantly, the former TFC membranes can achieve effective separation of dye mixtures with similar molecular weight based on their charge and strict molecular size. We demonstrate that molecular-level structural design of IP monomers have tremendous potential for the fabrication of high performance OSN membranes with potential industrial applications.

Results and Discussion

Construction of nanofilms by interfacial polymerization

Amino-BIPOL was synthesized in two steps from 2,2’-biphenol (BIPOL), its chemical structure was confirmed by ^{1}H NMR/^{13}C NMR analysis. Hydroxyl-BIPOL was synthesized using previously published methodology with some small modifications.[21] Synthetic details are provided in the Supporting Information. We designed and employed BIPOL derivatives as the sole aqueous monomer to form nanofilms *in situ* due to their multi-functionality, ionizable nature in water, short length between the reactive sites and rotatable non-coplanar configuration of two phenyl groups. Aromatic polyesteramide or polyester nanofilms were obtained by reacting the appropriate BIPOL monomers in water at the interface with an organic phase of Isopar G containing trimesoyl chloride (TMC) as shown in Figure 1. The polymerization reaction between monomers containing ‘4+3’ functional groups ensured the nanofilms have a highly cross-linked network structure with good tolerance towards various

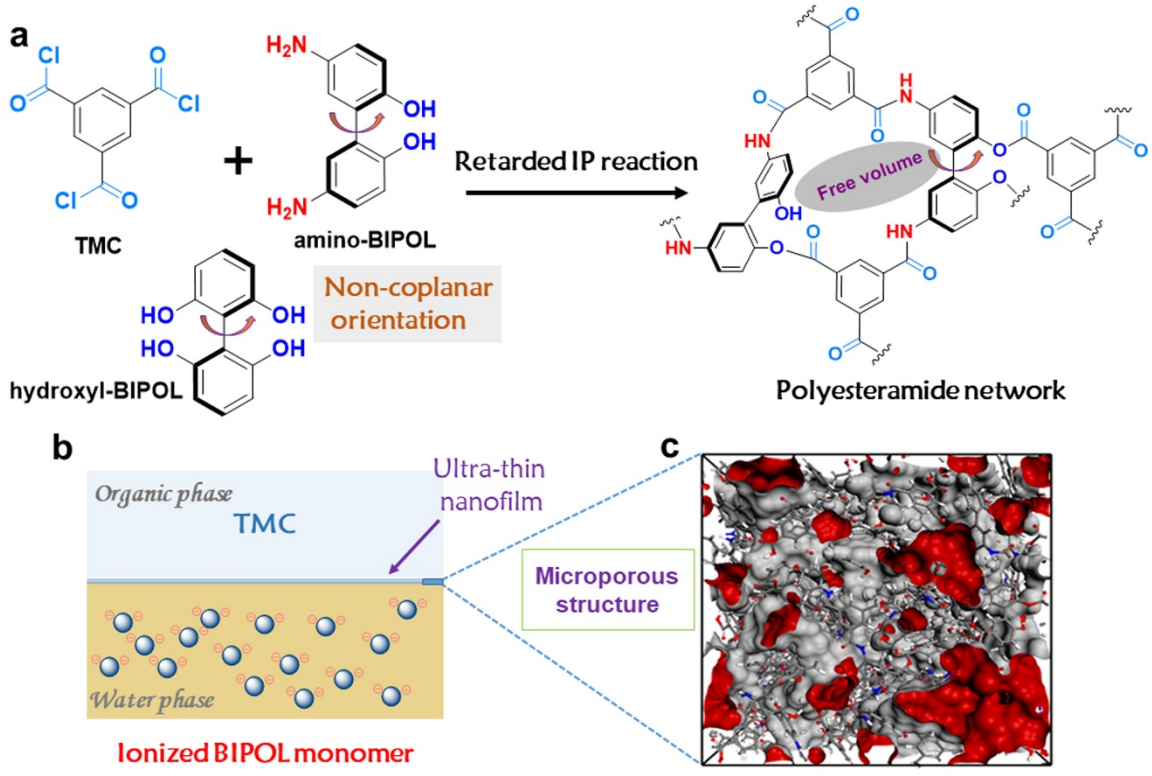

Figure 1. Interfacial synthesis of the polyesteramide/polyester nanofilms. a) The chemical structure and schematic illustrations of the amino-BIPOL, hydroxyl-BIPOL, TMC and the resulted polyesteramide networks. b) Diagram of the IP reaction to afford microporous polyesteramide/polyester nanofilm with TMC in the organic phase and amino-BIPOL/hydroxyl-BIPOL in the aqueous phase. c) Illustration of the free volume of the resulting polyesteramide nanofilm derived from dynamic simulaion. The gray shading indicates the voids in the membrane models detected by a probe with the radius of 1.0 Å and the openings to the voids are displayed in red.

organic solvents as demonstrated by their unchanged properties after 30 days immersion in various solvents (Figure S4). The results for molecular dynamic simulation helps to visualise the microporous structure of the polyesteramide nanofilm (Figure 1c).

As depicted in Figure 2a-b and Figure S5, a free-standing polyesteramide nanofilm was formed at the water/organic interface, which could be isolated and supported by a wire loop. SEM images of Figure 2c-d supported on a porous alumina substrate showed the ultra-thin, continuous, defect-free structure of the nanofilm. Its robustness allowed collection by suction with a pipette without visible tear, which then could spread out evenly at the surface of water (Video S1). The amino-BIPOL composite membranes were fabricated directly onto a PAN ultrafiltration support and demonstrated by SEM images (Figure 2f and Figures S6-8). A smooth and defect-free surface could be observed with the original porous substrate being fully covered by the polyesteramide layer. Atomic force microscopy (AFM) of the free-standing nanofilms on a silica wafer revealed that the film thickness increases gradually with the IP reaction duration (Figure 2g-h and Figure S9). The film thickness is as low as ~5 nm at reaction time of 1 min, while increases to ~45 nm at 10 min. The roughness of films also shows a slight gradual increase with root mean square roughness (Rq) from 1.87 nm to 5.25 nm, which are consist with the SEM results. In addition, spectroscopic ellipsometry (SE) gives similar values of film thickness at different reaction duration (Figure 2i). For the cross-sectional SEM images of the composite membranes, it is difficult to clearly identify the boundary between the thin polyester/amide layer and the PAN substrate for fabrication using shorter IP reaction times. Nevertheless, for the reaction time of 10 min a film thickness value in the range of 45-51 nm can be easily measured (Figures S7 and 8). The thickness of the active layer of the composite membrane (IP 10 min) is consist with that of the free-standing nanofilm prepared at the organic/water interface with similar IP parameters. For the polyester membranes based on hydroxyl-BIPOL, the nanofilm thickness increases from ~14 nm at IP reaction time of 1 min to ~65 nm at 10 min. SEM images show defect-free nanofilms formed on the PAN substrate. The value of polyester

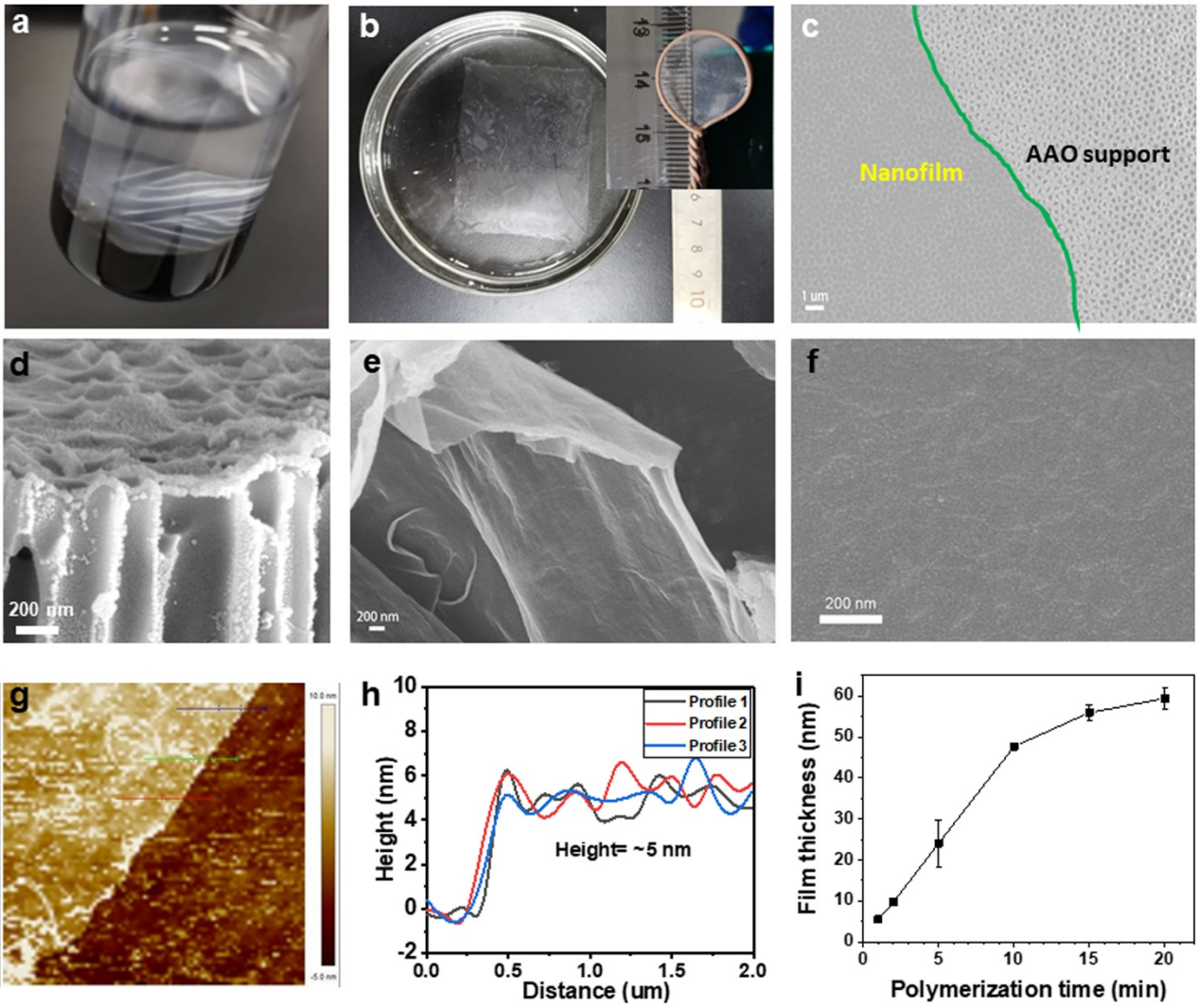

Figure 2. Morphologies characterizations of polyesteramide nanofilms. a-b) Photographs of the free-standing polysteramide nanofilm formed at the free organic/water interface, floating in water and captured by a wire loop. c-d) SEM of the top-view and cross-section images of the free-standing polyesteramide nanofilms on porous AAO substrate. e-f) SEM surface images of the nanofilm powder synthesized through IP under rigorous stirring, and the amino-BIPOL/PAN composite membrane. g-h) AFM images and corresponding height profile of the free-standing nanofilm (IP 1 min) on top of a silicon wafer. i) film thickness varies with the IP reaction duration monitored by spectroscopic ellipsometry (SE).

nanofilm thickness from cross-sectional SEM images (IP 10 min) is also consistent with that obtained from SE data (Figures S10-13).

Combining SEM and SE data with that from solvent flux for the composite membranes prepared from each of these two monomers using similar reaction times (Figures S26a and 27a), it can be deduced that the active layer of the composite membranes is of similar thickness to that of the equivalent free-standing nanofilm. Conventional IP monomers, such as *meta*-phenylenediamine (MPD) and piperazine (PIP) exhibited quite distinct IP properties with different nanofilm thickness obtained when reacted with TMC at the free organic/water interface or on various porous supports.[6, 22] Hence, in order to achieve an ultra-thin (less than 10 nm) PA layer, the construction of a special interface on the substrate is required, such as applying nanostrands to form a sacrificial interlayer.[7] In contrast, for IP of the BIPOL monomers with TMC, simple control over the reaction duration can easily provide hypercross-linked nanofilms of less than 5 nm thickness, which is attractive for OSN membrane fabrication. This IP behaviour can be attributed to the highly ionized nature of the phenol moieties on the BIPOL monomers and their relatively large molecular size compared to MPD and PIP, which will reduce the diffusion rate of monomers to the organic/water interface, therefore giving a 'retarded' IP reaction.[12b]

Membrane characterization and structure simulation

The structure of the nanofilms was probed by FT-IR spectroscopy and X-ray photoelectron spectroscopy (XPS). For FT-IR, the peaks at 1732, 1654 cm^{-1} and 1548 cm^{-1} for the polyesteramide nanofilm could be ascribled to the ester and amide C=O groups. The hydroxyl-BIPOL derived nanofilms show a strong adsorption peak at 1741 cm^{-1} associated with the expected ester bonds (Figure 3a and Figure S14). XPS analysis was consistent with the expected chemical compositions of the composite membranes and the nanofilm (Figure 3b-e and Figures S15 and 16). Thermal analysis demonstrates that the BIPOL nanofilms are stable up to 300 °C under nitrogen atmosphere (Figure 3f). The BIPOL/TMC composite membranes exhibit moderate hydropilicity with water contact angles of around 70° and 60°, respectively (Figure S17). Streaming potential analysis indicated an amphoteric character with the surface charge of ~-36 mV/-32 mV at neutral pH (Figure S18).

CO_2 adsorption isotherms of the BIPOL/TMC nanofilms at 273 K are consistent with significant microporosity with accessible surface area of 133 or 94 $m^2\ g^{-1}$ for nanofilms of amino-BIPOL and hydroxyl-BIPOL, respectively with pore size distribution for both in the range of 0.50-0.90 nm, in which hydroxyl-BIPOL nanofilm possessing more large micropores than amino-BIPOL nanofilm (Figure 4a). These accessible surface area are about 2-fold that of the reported MPD/TMC powder (with value of 49 $m^2\ g^{-1}$), similar IP polyamides.[15a] X-ray diffraction (XRD) analysis shows typical amorphous scattering for the polyesteramide/ polyester nanofilms with a *d*-spacing of about 0.416/0.406 nm, indicating small aperture size (Figure S20).

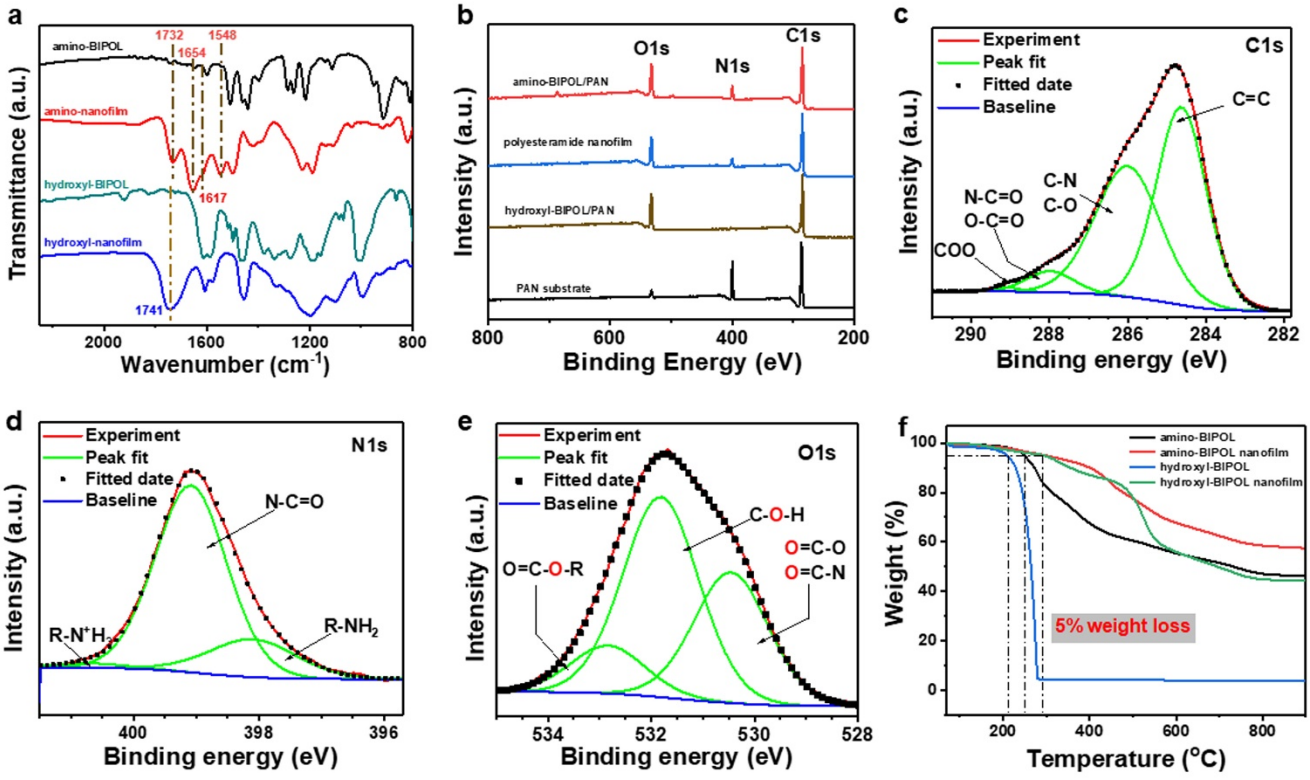

Figure 3. Chemical structure characterization of the nanofilms. a) FT-IR spectra of the BINOL monomers and the resulting nanofilms. b) XPS survey spectra of PAN substrate, polyesteramide nanofilm, hydroxyl-BIPOL and amino-BIPOL/PAN composite membrane. c) XPS narrow scan spectra of C1s spectra, d) N1s spectra and e) O1s spectra of the polyesteramide nanofilm. f) TGA curves for monomers BIPOL and the polyesteramide/polyester nanofilm.

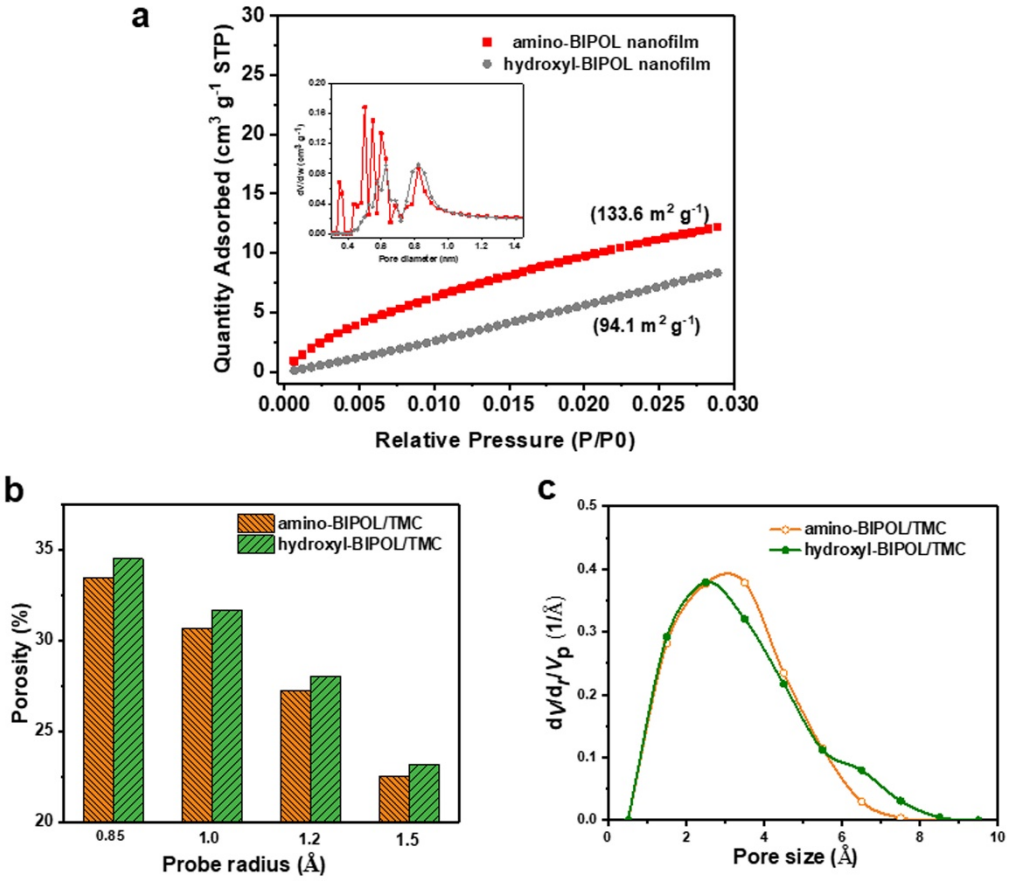

Figure 4. Polymer structural analysis. a) CO_2 adsorption isotherms of amino-BIPOL/TMC nanofilm and hydroxyl-BIPOL/TMC nanofilm measured at 273 K, the insert denotes pore size distribution employing the nonlocal density functional theory (NLDFT). Molecular modeling. b) Comparison of porosity measured by different sizes of probes. c) Simulated pore size (diameter) distribution for two membrane models.

Molecular simulation generated structural models of the porosity of the amorphous polymer networks for the two BIPOL/TMC nanofilms, with simulation parameters and detailed results provided in the Supporting Information (Table S2 and Figures S21-25). The Figure S23 exhibits the free volume snapshots in relation to different sizes of probes for corresponding cell volumes of ~40 nm^3. Analysis probe radius of 0.85 to 1.2 Å demonstrates that the hydroxyl-BIPOL derived nanofilm is more porous than the corresponding amino-BIPOL polymer (Figure 4b). In addition, the hydroxyl-BIPOL polymer possesses a distinct fraction of micropores in range of 0.6-0.8 Å (Figure 4c). In comparison, the pore size values derived from the simulated model are relatively smaller than the real diameters revealed by the CO_2 adsorption experiment, which should be because of the leaving out of organic solvent factors in the simulated model as observed in the polyarylate membrane[15b] and the all-rigid CMPs[13c] membranes. These simulated values for porosity are consistent with the performances of the two types of OSN membranes as reported below.

Separation performance of composite membranes

The performance of the composite membranes derived from amino-BIPOL or hydroxyl-BIPOL are shown in Figure 5a-b and Figures S26 and 27. For the membrane derived from amino-BIPOL with an IP reaction time of 1 min, water and methanol permeances are high with values of 17.6 LMH/bar and 13.0 LMH/bar, respectively. Those derived from hydroxyl-BIPOL provide even higher pemeances of 25.2 LMH/bar and 17.2 LMH/bar, respectively. Film permeances decrease sharply with longer reaction durations (1-10 min) correlating with increases in film thickness over this (Figure 2i and Figures S9 and 13). Importantly, the solute rejection performance of the amino-BIPOL membranes proved to be independent of reaction duration, indicating that dense selective layers have formed even at an IP reaction duration of only 1 min (Figure S26b). For the membranes derived from hydroxyl-BIPOL, the rejection performance was enhanced slightly by reaction time, indicating a looser packing of the network than that derived from amino-BIPOL, which would possess greater H-bonding characteristics (Figure S27b). As displayed in Figure S28, the pure solvent permeance of the two BIPOL composite membranes linearly correlated with the combined solvent parameters (the solvent solubility, viscosity, and molecular diameter). That phenomenon was first disclosed by Livingston et al.[7], and could be used to well predict the solvent permeance of PA TFC membranes prepared by IP technology. The separation performance of amino-BIPOL/PAN composite membranes was compared with our lab-made MPD/PAN membrane prepared under the similar conditions (Figure S30). The replacement of MPD by amino-BIPOL elevated the methanol permeance by ~5-fold whilst increasing rejection of methyl orange (MO, 327 Da) from 95.2 to 97.5%.

The amino-BIPOL/PAN composite membranes exhibit excellent rejection of most dye molecules, with a MWCO as low as 233 Da in methanol, for example, maintaining 96.3% rejection of the neutral dye methyl red (Mw = 269 Da). The rejection of neutral small sugars and glycerol in aqueous solution was also demonstrated for the composite membranes (Figures S31 and 32). MWCO of 170 Da and 295 Da, with an effective pore radius of 0.187 nm and 0.204 nm for amino-BIPOL and hydroxyl-BIPOL membranes, respectively, was demonstrated, which are smaller compared with that determined in methanol. This difference may be due to the hydration effect of sugar molecules in aqueous solution and/or greater swelling of the membrane in methanol. The lower selectivity of membrane hydroxyl-BIPOL as compared to membrane amino-BIPOL likely due to less hydrogen bonding within the formed network polymer. The long-term operation performances of the amino-BIPOL/PAN membrane (IP 1 min) was challenged by alternating water, methanol, ethanol and THF within a duration of 120 h, in addition to methyl orange (MO) and sudan orange G (SOG) methanol solution filtration experiments lasting for 80 h (Figures S33 and 34). These results fully confirm the robustness and stability of the polyester/amide composite membrane. The inorganic salts rejection abilities of the membrane were also evaluated showing a high sodium sulfate rejection of 97.5% and low sodium chloride rejection of 21.9%, with a high mono/divalent salt selectivity (Figure S35).

The OSN separation performance of BIPOL/PAN composite membranes was further evaluated by comparison with the trade-off of permance/selectivity for recently reported advanced OSN membranes (Figure 5c and Table S5). The BIPOL-based membranes outperform most of the recently-reported advanced OSN membranes, except for the sub-10 nm polyamide nanofilms on AAO support activated by DMF.[7] The selectivity of the amino-BIPOL/PAN membrane significantly exceeds that of four kinds of conjugated microporous polymers (CMPs) membranes,[13] polyester-CD[12a, 23] and polyamide-CD membrane,[24] whilst providing a high MeOH permeance of 13 LMH/bar. Importantly, most of the reported OSN membranes exhibit low or moderate selectivities for small organic solutes, usually with MWCO larger than 350 Da and thus would have only limited extensive applications for future industrial OSN processes.

To verify the molecular sieving capability of the BIPOL-based composite membrane, the separation of a mixed solution of methyl orange (MO, 327 Da) and methylene blue (MB, 320 Da) was achieved. It could be observed that the MO (high rejection of 97.5%) was almost fully retained by the amino-BIPOL membrane, while MB (low rejection of ~60%) passed through membrane to give a blue filtrate solution. This precise separation was quantified by UV-vis spectroscopy (Figure 5d-e). The selective mechanism should be on account of the negatively charged surface of amino-BIPOL membrane (Figure S18), enhancing retention of the negatively charged MO. Furthermore, the amino-BIPOL membrane in this study exhibited not only charge-selective but also strict size-selective characteristics, as neutral dye methyl red (MR, 269 Da) and positive-charged dye crystal violet (CV, 408 Da) both have high rejection values (>96%).

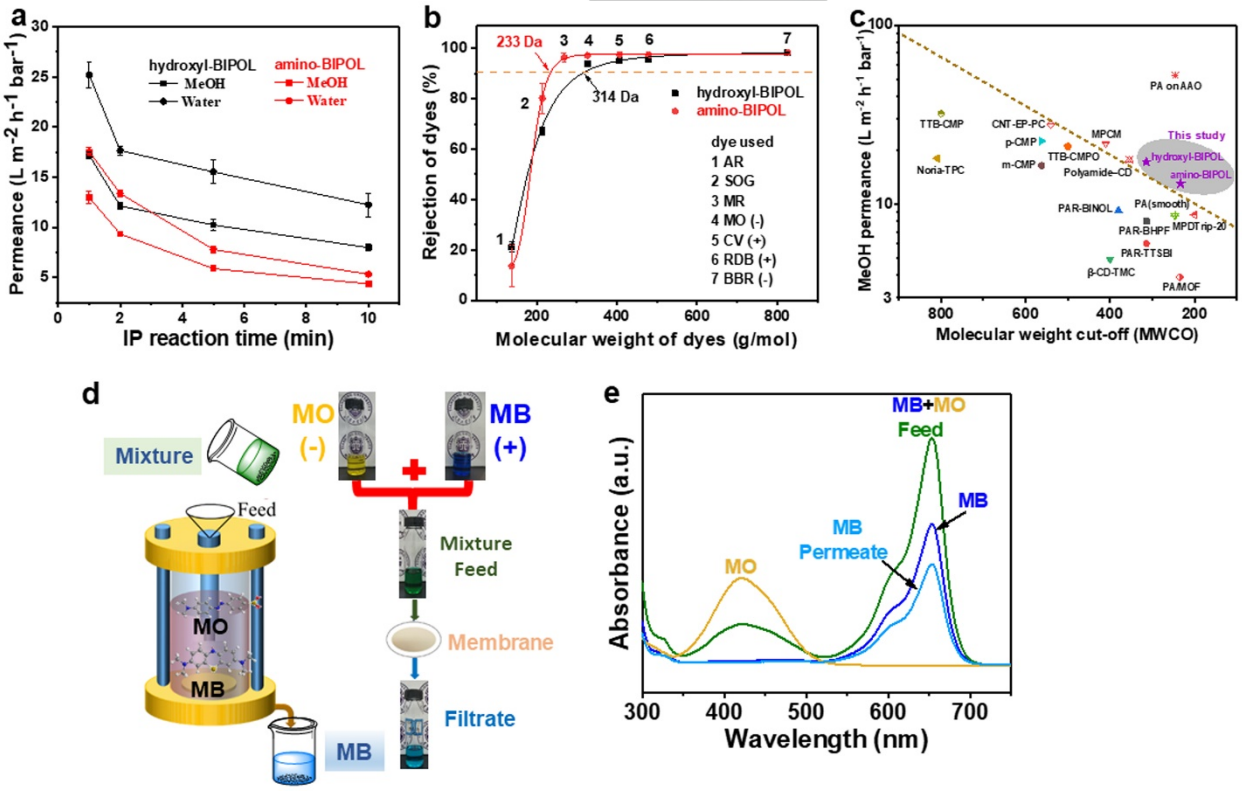

Figure 5. Separation performance. a) Methanol and water permeances of the fabricated BIPOL/PAN composite membranes with different IP reaction time. b) Rejections behavior versus selected dyes with different molecular weight in methanol solution by the fabricated composite membranes with a IP reaction time of 1 min. c) Permeselectivity comparision of the two BIPOL/PAN membranes with the state-of-the-art OSN membranes. d) Schematic illustration and e) UV-Vis adsorption spectra of the methyl organge (MO, 327 Da) and methylene blue (MB, 320 Da) mixture in methanol before and after filtration through amino-BIPOL/PAN composite membranes to evidence of its precise molecular sieving separation performance.

Conclusion

In summary, here we described the molecular level design of IP monomers for the construction ultrathin nanofilms with enhanced microporosity, based on the multi-functional BIPOL derivatives. We noted that the resulting composite membranes show high solvent resistance and outstanding perm-selectivity performances in OSN process, which exceed most of the reported advanced polymeric membranes. The microstructures of the polymeric networks were further revealed by the CO_2 adsorption experiment and molecular dynamic simulations. In addition, precise separation of small dye mixtures of MO and MB with similar molecular weights based on both their charge and molecular size are achieved. Overall, this study has demonstrated that 2,2'-biphenol derivatives are excellent monomers for high performance OSN membranes fabricated via a standard IP process suitable for industrial-scale production. Other biphenyl analogues for the construction of OSN membranes are being studied in our laboratory.

Acknowledgements

The authors would like to thank the Analytical & Testing Center of Tiangong University for XPS, NMR and AFM characterization. And we also gratefully acknowledge the support of National Natural Science Foundation of China (No. 21978215), Tianjin Education Scientific Research Projects (No. 2019KJ006), the Science and Technology Plans of Tianjin (No. 20ZYJDJC00100), and the Natural Science Foundation of Tianjin (No. 18JCYBJC43300). S.-L. was supported in part by the China Scholarship Council.

Conflict of Interest

The authors declare no conflict of interest.

Keywords: Microporous organic polymers (MOPs) • Organic solvent nanofiltration • Interfacial polymerization • 2,2'-Biphenol derivative monomer • Precise sieving

[1] a) M. S. Mauter, I. Zucker, F. Perreault, J. R. Werber, J.-H. Kim, M. Elimelech, *Nat. Sustain.* **2018**, *1*, 166-175; b) J. R. Werber, C. O. Osuji, M. Elimelech, *Nat. Rev. Mater.* **2016**, *1*, 16018; c) S. P. Nunes, P. Z. Culfaz-Emecen, G. Z. Ramon, T. Visser, G. H. Koops, W. Jin, M. Ulbricht, *J. Membr. Sci.* **2020**, *598*, 117761.

[2] a) K. A. Thompson, R. Mathias, D. Kim, J. Kim, N. Rangnekar, J. R. Johnson, S. J. Hoy, I. Bechis, A. Tarzia, K. E. Jelfs, B. A. McCool, A. G. Livingston, R. P. Lively, M. G. Finn, *Science* **2020**, *369*, 310-315; b) K. S. Goh, Y. Chen, J. Y. Chong, T. H. Bae, R. Wang, *J. Membr. Sci.* **2021**, *621*, 119008; c) P. Marchetti, M. F. Jimenez Solomon, G. Szekely, A. G. Livingston, *Chem. Rev.* **2014**, *114*, 10735-10806; d) X. Shui, J. Li, M. Zhang, C. Fang, L. Zhu, *J. Membr. Sci.* **2021**, *628*, 119249; e) M. Amirilargani, M. Sadrzadeh, E. J. R. Sudhölter, L. C. P. M. de Smet, *Chem. Eng. J.* **2016**, *289*, 562-582; f) K. Tiwari, S. Modak, P. Sarkar, S. Ray, V. Adupa, K. A. Reddy, S. K. Pramanik, A. Das, S. Karan, *iScience* **2022**, *25*, 104027.

[3] a) D. Zhao, J. F. Kim, G. Ignacz, P. Pogany, Y. M. Lee, G. Szekely, *ACS Nano* **2019**, *13*, 125-133; b) B. Liang, X. He, J. Hou, L. Li, Z. Tang, *Adv. Mater.* **2019**, *31*, 1806090; c) P. He, S. Zhao, C. Mao, Y. Wang, G. Ma, Z. Wang, J. Wang, *Chem. Eng. J.* **2021**, *420*, 129338; d) G. M. Shi, Y. Feng, B. Li, H. M. Tham, J.-Y. Lai, T.-S. Chung, *Prog. Polym. Sci.* **2021**, *123*, 101470; e) Y. Li, Z. Guo, S. Li, B. Van der Bruggen, *Adv. Mater. Interfaces* **2021**, *8*, 2001671.

[4] a) Y. Li, J. Zhu, S. Li, Z. Guo, B. Van der Bruggen, *ACS Appl. Mater. Interfaces* **2020**, *12*, 31962–31974; b) Y. Li, E. Wong, A. Volodine, C. Van Haesendonck, K. Zhang, B. Van der Bruggen, *J. Mater. Chem. A* **2019**, *7*, 19269-19279; c) J. Liu, S. Wang, T. Huang, P. Manchanda, E. Abou-Hamad, S. P. Nunes, *Sci. Adv.* **2020**, *6*, eabb3188.

[5] a) J. Zhu, S. Yuan, J. Wang, Y. Zhang, M. Tian, B. Van der Bruggen, *Prog. Polym. Sci.* **2020**, *110*, 101308; b) B. Li, S. Japip, T.-S. Chung, *Nat. Commun.* **2020**, *11*, 1198; c) C. Liu, J. Yang, B.-B. Guo, S. Agarwal, A. Greiner, Z.-K. Xu, *Angew. Chem., Int. Ed.* **2021**, *60*, 14636-14643; d) A. He, Z. Jiang, Y. Wu, H. Hussain, J. Rawle, M. E. Briggs, M. A. Little, A. G. Livingston, A. I. Cooper, *Nat. Mater.* **2022**, *21*, 463–470.

[6] J. Zhiwei, K. Santanu, L. A. G., *Adv. Mater.* **2018**, *30*, 1705973.

[7] S. Karan, Z. Jiang, A. G. Livingston, *Science* **2015**, *348*, 1347-1351.

[8] S. Karan, S. Samitsu, X. Peng, K. Kurashima, I. Ichinose, *Science* **2012**, *335*, 444-447.

[9] C. Li, S. Li, L. Tian, J. Zhang, B. Su, M. Z. Hu, *J. Membr. Sci.* **2019**, *572*, 520-531.

[10] a) X. Guo, D. Liu, T. Han, H. Huang, Q. Yang, C. Zhong, *AIChE J.* **2017**, *63*, 1303-1312; b) S. Sorribas, P. Gorgojo, C. Téllez, J. Coronas, A. G. Livingston, *J. Am. Chem. Soc.* **2013**, *135*, 15201-15208; c) Y. Zhang, X. Cheng, X. Jiang, J. J. Urban, C. H. Lau, S. Liu, L. Shao, *Mater. Today* **2020**, *36*, 40-47.

[11] Q. Liu, S. J. D. Smith, K. Konstas, D. Ng, K. Zhang, M. R. Hill, Z. Xie, *J. Membr. Sci.* **2021**, *620*, 118911.

[12] a) J. Liu, D. Hua, Y. Zhang, S. Japip, T.-S. Chung, *Adv. Mater.* **2018**, *30*, 1705933; b) T. Huang, B. A. Moosa, P. Hoang, J. Liu, S. Chisca, G. Zhang, M. AlYami, N. M. Khashab, S. P. Nunes, *Nat. Commun.* **2020**, *11*, 5882.

[13] a) Z. Zhou, X. Li, D. Guo, D. B. Shinde, D. Lu, L. Chen, X. Liu, L. Cao, A. M. Aboalsaud, Y. Hu, Z. Lai, *Nat. Commun.* **2020**, *11*, 5323; b) X. He, H. Sin, B. Liang, Z. A. Ghazi, A. M. Khattak, N. A. Khan, H. R. Alanagh, L. Li, X. Lu, Z. Tang, *Adv. Funct. Mater.* **2019**, *29*, 1900134; c) B. Liang, H. Wang, X. Shi, B. Shen, X. He, Z. A. Ghazi, N. A. Khan, H. Sin, A. M. Khattak, L. Li, Z. Tang, *Nat. Chem.* **2018**, *10*, 961–967.

[14] a) D. B. Shinde, G. Sheng, X. Li, M. Ostwal, A.-H. Emwas, K.-W. Huang, Z. Lai, *J. Am. Chem. Soc.* **2018**, *140*, 14342-14349; b) Z. Wang, Q. Yu, Y. Huang, H. An, Y. Zhao, Y. Feng, X. Li, X. Shi, J. Liang, F. Pan, P. Cheng, Y. Chen, S. Ma, Z. Zhang, *ACS Central Science* **2019**, *5*, 1352–1359; c) L. Shen, Q. Shi, S. Zhang, J. Gao, D. C. Cheng, M. Yi, R. Song, L. Wang, J. Jiang, R. Karnik, S. Zhang, *Sci. Adv.* **2021**, *7*, eabg6263.

[15] a) Z. Ali, B. S. Ghanem, Y. Wang, F. Pacheco, W. Ogieglo, H. Vovusha, G. Genduso, U. Schwingenschlögl, Y. Han, I. Pinnau, *Adv. Mater.* **2020**, *32*, 2001132; b) M. F. Jimenez-Solomon, Q. Song, K. E. Jelfs, M. Munoz-Ibanez, A. G. Livingston, *Nat. Mater.* **2016**, *15*, 760-767.

[16] M. L. Jue, D.-Y. Koh, B. A. McCool, R. P. Lively, *Chem. Mater.* **2017**, *29*, 9863-9876.

[17] M. J. Baran, M. E. Carrington, S. Sahu, A. Baskin, J. Song, M. A. Baird, K. S. Han, K. T. Mueller, S. J. Teat, S. M. Meckler, C. Fu, D. Prendergast, B. A. Helms, *Nature* **2021**, *592*, 225-231.

[18] D. Jiao, W. Zhi, L. Xu, W. Jixiao, *CIESC Journal* **2020**, *71*, 4885-4902.

[19] W. Fu, W. Zhang, H. Chen, S.-L. Li, W. Shi, Y. Hu, *J. Mater. Chem. A* **2021**, *9*, 7180-7189.

[20] a) N. B. McKeown, *Polymer* **2020**, *202*, 122736; b) Z. Zuo, R. S. Kim, D. A. Watson, *J. Am. Chem. Soc.* **2021**, *143*, 1328-1333; c) G. Storch, O. Trapp, *Nat. Chem.* **2017**, *9*, 179-187.

[21] C.-Y. Lee, C.-H. Cheon, *Adv. Synth. Catal.* **2016**, *358*, 549-554.

[22] Y. Li, X. You, Y. Li, J. Yuan, J. Shen, R. Zhang, H. Wu, Y. Su, Z. Jiang, *J. Mater. Chem. A* **2020**, *8*, 23930-23938.

[23] L. F. Villalobos, T. Huang, K.-V. Peinemann, *Adv. Mater.* **2017**, *29*, 1606641.

[24] T. Huang, T. Puspasari, S. P. Nunes, K.-V. Peinemann, *Adv. Funct. Mater.* **2020**, *30*, 1906797.

Entry for the Table of Contents

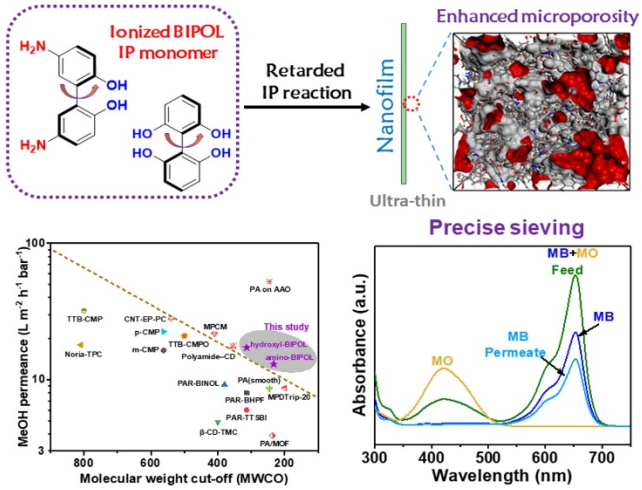

Ultra-thin microporous polymer composite membranes with extraordinary perm-selectivity for organic solvent nanofiltration were fabricated by employing two novel 2,2'-biphenol (BIPOL) derivatives as interfacial polymerization aqueous monomer. The enhanced microporosity arisis from the hyper-crosslinked network structure and monomer rigidity. Moreover, it can achieve precise separation of organic molecules with similar molecular weights on their charge and molecular size.